

Mark D Does

List of Publications by Year in descending order

Source: <https://exaly.com/author-pdf/8474610/publications.pdf>

Version: 2024-02-01

103
papers

4,654
citations

71061

41
h-index

114418

63
g-index

103
all docs

103
docs citations

103
times ranked

4936
citing authors


#	ARTICLE	IF	CITATIONS
1	Multi-compartment microscopic diffusion imaging. <i>NeuroImage</i> , 2016, 139, 346-359.	2.1	280
2	Changes in water diffusion due to Wallerian degeneration in peripheral nerve. <i>Magnetic Resonance in Medicine</i> , 1996, 36, 627-631.	1.9	248
3	The Role of Water Compartments in the Material Properties of Cortical Bone. <i>Calcified Tissue International</i> , 2015, 97, 292-307.	1.5	180
4	Characterization of ^1H NMR signal in human cortical bone for magnetic resonance imaging. <i>Magnetic Resonance in Medicine</i> , 2010, 64, 680-687.	1.9	135
5	Characterization of tissue structure at varying length scales using temporal diffusion spectroscopy. <i>NMR in Biomedicine</i> , 2010, 23, 745-756.	1.6	131
6	Iron, Myelin, and the Brain: Neuroimaging Meets Neurobiology. <i>Trends in Neurosciences</i> , 2019, 42, 384-401.	4.2	123
7	Mapping mean axon diameter and axonal volume fraction by MRI using temporal diffusion spectroscopy. <i>NeuroImage</i> , 2014, 103, 10-19.	2.1	109
8	Clinically compatible MRI strategies for discriminating bound and pore water in cortical bone. <i>Magnetic Resonance in Medicine</i> , 2012, 68, 1774-1784.	1.9	107
9	Optimizing pulsed chemical exchange saturation transfer imaging sequences. <i>Magnetic Resonance in Medicine</i> , 2011, 66, 1100-1108.	1.9	105
10	A new method for detecting exchanging amide protons using chemical exchange rotation transfer. <i>Magnetic Resonance in Medicine</i> , 2013, 69, 637-647.	1.9	105
11	The radial diffusivity and magnetization transfer pool size ratio are sensitive markers for demyelination in a rat model of type III multiple sclerosis (MS) lesions. <i>NeuroImage</i> , 2013, 74, 298-305.	2.1	104
12	Non-invasive Predictors of Human Cortical Bone Mechanical Properties: T2-Discriminated ^1H NMR Compared with High Resolution X-ray. <i>PLoS ONE</i> , 2011, 6, e16359.	1.1	104
13	Origins of the ultrashort T_2 ^1H NMR signals in myelinated nerve: A direct measure of myelin content?. <i>Magnetic Resonance in Medicine</i> , 2011, 66, 24-31.	1.9	99
14	Identifying Novel Clinical Surrogates to Assess Human Bone Fracture Toughness. <i>Journal of Bone and Mineral Research</i> , 2015, 30, 1290-1300.	3.1	94
15	Multixponential T_2 relaxation in degenerating peripheral nerve. <i>Magnetic Resonance in Medicine</i> , 1996, 35, 207-213.	1.9	91
16	Inferring brain tissue composition and microstructure via MR relaxometry. <i>NeuroImage</i> , 2018, 182, 136-148.	2.1	87
17	Effect of intercompartmental water exchange on the apparent myelin water fraction in multixponential T_2 measurements of rat spinal cord. <i>Magnetic Resonance in Medicine</i> , 2012, 67, 793-800.	1.9	84
18	Multi-angle ratiometric approach to measure chemical exchange in amide proton transfer imaging. <i>Magnetic Resonance in Medicine</i> , 2012, 68, 711-719.	1.9	79

#	ARTICLE	IF	CITATIONS
19	Multi-component T1 relaxation and magnetisation transfer in peripheral nerve. <i>Magnetic Resonance Imaging</i> , 1998, 16, 1033-1041.	1.0	78
20	The microstructural correlates of T ₁ in white matter. <i>Magnetic Resonance in Medicine</i> , 2016, 75, 1341-1345.	1.9	74
21	Multi-parametric MRI characterization of healthy human thigh muscles at 3.0 T - relaxation, magnetization transfer, fat/water, and diffusion tensor imaging. <i>NMR in Biomedicine</i> , 2014, 27, 1070-1084.	1.6	71
22	Evaluation of diffusion kurtosis imaging in ex vivo hypomyelinated mouse brains. <i>NeuroImage</i> , 2016, 124, 612-626.	2.1	71
23	On the inherent precision of mcDESPOT. <i>Magnetic Resonance in Medicine</i> , 2013, 69, 127-136.	1.9	70
24	Evaluating g-ratio weighted changes in the corpus callosum as a function of age and sex. <i>NeuroImage</i> , 2018, 182, 304-313.	2.1	68
25	Imaging amide proton transfer and nuclear overhauser enhancement using chemical exchange rotation transfer (CERT). <i>Magnetic Resonance in Medicine</i> , 2014, 72, 471-476.	1.9	62
26	Compartmental study of diffusion and relaxation measured in vivo in normal and ischemic rat brain and trigeminal nerve. <i>Magnetic Resonance in Medicine</i> , 2000, 43, 837-844.	1.9	58
27	In Vivo Quantitative MR Imaging of Bound and Pore Water in Cortical Bone. <i>Radiology</i> , 2015, 277, 221-229.	3.6	58
28	Myelin volume fraction imaging with MRI. <i>NeuroImage</i> , 2018, 182, 511-521.	2.1	58
29	Optimized inversion recovery sequences for quantitative <i>T₁</i> and magnetization transfer imaging. <i>Magnetic Resonance in Medicine</i> , 2010, 64, 491-500.	1.9	57
30	Insights into reference point indentation involving human cortical bone: Sensitivity to tissue anisotropy and mechanical behavior. <i>Journal of the Mechanical Behavior of Biomedical Materials</i> , 2014, 37, 174-185.	1.5	57
31	New Insights into Tumor Microstructure Using Temporal Diffusion Spectroscopy. <i>Cancer Research</i> , 2008, 68, 5941-5947.	0.4	56
32	Partial removal of pore and loosely bound water by low-energy drying decreases cortical bone toughness in young and old donors. <i>Journal of the Mechanical Behavior of Biomedical Materials</i> , 2013, 22, 136-145.	1.5	56
33	Characterizing inter-compartmental water exchange in myelinated tissue using relaxation exchange spectroscopy. <i>Magnetic Resonance in Medicine</i> , 2013, 70, 1450-1459.	1.9	55
34	MRI-derived bound and pore water concentrations as predictors of fracture resistance. <i>Bone</i> , 2016, 87, 1-10.	1.4	54
35	Advances in imaging approaches to fracture risk evaluation. <i>Translational Research</i> , 2017, 181, 1-14.	2.2	54
36	Hypomyelination following deletion of <i>Tsc2</i> in oligodendrocyte precursors. <i>Annals of Clinical and Translational Neurology</i> , 2015, 2, 1041-1054.	1.7	53

#	ARTICLE	IF	CITATIONS
37	Evaluation of principal component analysis image denoising on multi-exponential MRI relaxometry. <i>Magnetic Resonance in Medicine</i> , 2019, 81, 3503-3514.	1.9	53
38	Validation of quantitative bound and pore water imaging in cortical bone. <i>Magnetic Resonance in Medicine</i> , 2014, 71, 2166-2171.	1.9	52
39	A revised model for estimating g-ratio from MRI. <i>NeuroImage</i> , 2016, 125, 1155-1158.	2.1	50
40	Multi-parametric MRI characterization of inflammation in murine skeletal muscle. <i>NMR in Biomedicine</i> , 2014, 27, 716-725.	1.6	49
41	Dipeptidyl peptidase IV deficiency increases susceptibility to angiotensin-converting enzyme inhibitor-induced peritracheal edema. <i>Journal of Allergy and Clinical Immunology</i> , 2007, 120, 403-408.	1.5	48
42	Modified oscillating gradient pulses for direct sampling of the diffusion spectrum suitable for imaging sequences. <i>Magnetic Resonance Imaging</i> , 2003, 21, 279-285.	1.0	47
43	Dependence of temporal diffusion spectra on microstructural properties of biological tissues. <i>Magnetic Resonance Imaging</i> , 2011, 29, 380-390.	1.0	40
44	Earlier detection of tumor treatment response using magnetic resonance diffusion imaging with oscillating gradients. <i>Magnetic Resonance Imaging</i> , 2011, 29, 315-323.	1.0	40
45	Characterizing Tumor Response to Chemotherapy at Various Length Scales Using Temporal Diffusion Spectroscopy. <i>PLoS ONE</i> , 2012, 7, e41714.	1.1	40
46	Transverse relaxation and magnetization transfer in skeletal muscle: Effect of pH. <i>Magnetic Resonance in Medicine</i> , 2009, 61, 560-569.	1.9	39
47	RF coil considerations for short T_2 MRI. <i>Magnetic Resonance in Medicine</i> , 2010, 64, 1652-1657.	1.9	39
48	Chemical exchange rotation transfer imaging of intermediate-exchanging amines at 2 Åpm. <i>NMR in Biomedicine</i> , 2017, 30, e3756.	1.6	39
49	Age-related changes in the fracture resistance of male Fischer F344 rat bone. <i>Bone</i> , 2016, 83, 220-232.	1.4	33
50	Influence of cell cycle phase on apparent diffusion coefficient in synchronized cells detected using temporal diffusion spectroscopy. <i>Magnetic Resonance in Medicine</i> , 2011, 65, 920-926.	1.9	32
51	Magnetic nanoparticles for imaging dendritic cells. <i>Magnetic Resonance in Medicine</i> , 2010, 63, 1383-1390.	1.9	29
52	Effects of intracellular organelles on the apparent diffusion coefficient of water molecules in cultured human embryonic kidney cells. <i>Magnetic Resonance in Medicine</i> , 2011, 65, 796-801.	1.9	28
53	Iterative Method for Predistortion of MRI Gradient Waveforms. <i>IEEE Transactions on Medical Imaging</i> , 2014, 33, 1641-1647.	5.4	25
54	The age-related decrease in material properties of BALB/c mouse long bones involves alterations to the extracellular matrix. <i>Bone</i> , 2020, 130, 115126.	1.4	25

#	ARTICLE	IF	CITATIONS
55	Fast and simplified mapping of mean axon diameter using temporal diffusion spectroscopy. <i>NMR in Biomedicine</i> , 2016, 29, 400-410.	1.6	24
56	Compartment-specific enhancement of white matter and nerve ex vivo using chromium. <i>Magnetic Resonance in Medicine</i> , 2010, 64, 688-697.	1.9	23
57	In-vivo multi-exponential T2, magnetization transfer and quantitative histology in a rat model of intramyelinic edema. <i>NeuroImage: Clinical</i> , 2013, 2, 810-817.	1.4	23
58	Loss of mTORC2 signaling in oligodendrocyte precursor cells delays myelination. <i>PLoS ONE</i> , 2017, 12, e0188417.	1.1	23
59	3D second bound and pore water concentration mapping of cortical bone using 2D UTE with optimized half-pulses. <i>Magnetic Resonance in Medicine</i> , 2017, 77, 945-950.	1.9	23
60	Quantitative analysis of mouse corpus callosum from electron microscopy images. <i>Data in Brief</i> , 2015, 5, 124-128.	0.5	21
61	Differences in sensitivity to microstructure between cyclic- and impact-based microindentation of human cortical bone. <i>Journal of Orthopaedic Research</i> , 2017, 35, 1442-1452.	1.2	21
62	Manipulating the Amount and Structure of the Organic Matrix Affects the Water Compartments of Human Cortical Bone. <i>JBMR Plus</i> , 2019, 3, e10135.	1.3	21
63	N,N-diethyldithiocarbamate promotes oxidative stress prior to myelin structural changes and increases myelin copper content. <i>Toxicology and Applied Pharmacology</i> , 2009, 239, 71-79.	1.3	19
64	Differential gene expression in the kidney of sickle cell transgenic mice: upregulated genes. <i>Blood Cells, Molecules, and Diseases</i> , 2003, 31, 370-380.	0.6	18
65	Measurement of APT using a combined CERT-AREX approach with varying duty cycles. <i>Magnetic Resonance Imaging</i> , 2017, 42, 22-31.	1.0	18
66	A novel technique using hydrophilic polymers to promote axonal fusion. <i>Neural Regeneration Research</i> , 2016, 11, 525.	1.6	18
67	Fast T ₂ mapping with multiple echo, caesar cipher acquisition and model-based reconstruction. <i>Magnetic Resonance in Medicine</i> , 2015, 73, 1065-1074.	1.9	17
68	A simple estimate of axon size with diffusion MRI. <i>NeuroImage</i> , 2021, 227, 117619.	2.1	17
69	Experimental studies of g-ratio MRI in ex vivo mouse brain. <i>NeuroImage</i> , 2018, 167, 366-371.	2.1	16
70	Relayed nuclear Overhauser enhancement sensitivity to membrane Cho phospholipids. <i>Magnetic Resonance in Medicine</i> , 2020, 84, 1961-1976.	1.9	16
71	Multicomponent T2 analysis of dithiocarbamate-mediated peripheral nerve demyelination. <i>NeuroToxicology</i> , 2007, 28, 645-654.	1.4	15
72	Diffusion time dependency along the human corpus callosum and exploration of age and sex differences as assessed by oscillating gradient spin-echo diffusion tensor imaging. <i>NeuroImage</i> , 2020, 210, 116533.	2.1	15

#	ARTICLE	IF	CITATIONS
73	Chemical exchange rotation transfer imaging of phosphocreatine in muscle. <i>NMR in Biomedicine</i> , 2021, 34, e4437.	1.6	15
74	Towards an analytic solution for pulsed CEST. <i>NMR in Biomedicine</i> , 2018, 31, e3903.	1.6	14
75	Chemical exchange rotation transfer (CERT) on human brain at 3 Tesla. <i>Magnetic Resonance in Medicine</i> , 2018, 80, 2609-2617.	1.9	14
76	A comparison of individual and population-derived vascular input functions for quantitative DCE-MRI in rats. <i>Magnetic Resonance Imaging</i> , 2014, 32, 397-401.	1.0	13
77	Comparison of dynamic contrast-enhanced MRI and quantitative SPECT in a rat glioma model. <i>Contrast Media and Molecular Imaging</i> , 2012, 7, 494-500.	0.4	12
78	Initial findings in traumatic peripheral nerve injury and repair with diffusion tensor imaging. <i>Annals of Clinical and Translational Neurology</i> , 2021, 8, 332-347.	1.7	12
79	Immediate Enhancement of Nerve Function Using a Novel Axonal Fusion Device After Neurotmesis. <i>Annals of Plastic Surgery</i> , 2017, 79, 590-599.	0.5	11
80	Optimization of DSC MRI Echo Times for CBV Measurements Using Error Analysis in a Pilot Study of High-Grade Gliomas. <i>American Journal of Neuroradiology</i> , 2017, 38, 1710-1715.	1.2	10
81	Diffusion Magnetic Resonance Imaging Predicts Peripheral Nerve Recovery in a Rat Sciatic Nerve Injury Model. <i>Plastic and Reconstructive Surgery</i> , 2020, 145, 949-956.	0.7	10
82	A GRM7 mutation associated with developmental delay reduces mGlu7 expression and produces neurological phenotypes. <i>JCI Insight</i> , 2021, 6, .	2.3	10
83	Relaxation-selective magnetization preparation based on T1 and T2. <i>Journal of Magnetic Resonance</i> , 2005, 172, 306-311.	1.2	8
84	A comparative assessment of preclinical chemotherapeutic response of tumors using quantitative non-Gaussian diffusion MRI. <i>Magnetic Resonance Imaging</i> , 2017, 37, 195-202.	1.0	8
85	Bridging the Gap. <i>Annals of Plastic Surgery</i> , 2017, 78, S328-S334.	0.5	8
86	Propagation of error from parameter constraints in quantitative MRI: Example application of multiple spin echo T_2 mapping. <i>Magnetic Resonance in Medicine</i> , 2018, 79, 673-682.	1.9	8
87	Noninvasive diffusion MRI to determine the severity of peripheral nerve injury. <i>Magnetic Resonance Imaging</i> , 2021, 83, 96-106.	1.0	8
88	Aqueous urea as a model system for bi-exponential relaxation. <i>Magnetic Resonance Materials in Physics, Biology, and Medicine</i> , 2007, 20, 51-56.	1.1	6
89	Simple and robust saturation-based slice selection for ultrashort echo time MRI. <i>Magnetic Resonance in Medicine</i> , 2015, 73, 2204-2211.	1.9	6
90	Assessment of the Effect of Autograft Orientation on Peripheral Nerve Regeneration Using Diffusion Tensor Imaging. <i>Annals of Plastic Surgery</i> , 2018, 80, 384-390.	0.5	6

#	ARTICLE	IF	CITATIONS
91	Microscopic susceptibility anisotropy imaging. <i>Magnetic Resonance in Medicine</i> , 2020, 84, 2739-2753.	1.9	6
92	Slice-selective extended phase graphs in gradient-crushed, transient-state free precession sequences: An application to MR fingerprinting. <i>Magnetic Resonance in Medicine</i> , 2020, 84, 3409-3422.	1.9	5
93	Quantitative T2 measurement of a single voxel with arbitrary shape using pinwheel excitation and CPMG acquisition. <i>Magnetic Resonance Materials in Physics, Biology, and Medicine</i> , 2007, 20, 233-240.	1.1	4
94	 $\int_0^1 \frac{1}{1+x^2} dx$ selective excitation pulse design using the Shinnar-Le Roux algorithm. <i>Journal of Magnetic Resonance</i> , 2014, 242, 189-196.	1.1	4
95	Quantitative Magnetic Resonance Imaging of Skeletal Muscle Disease. <i>Journal of Visualized Experiments</i> , 2016, . .	0.2	4
96	Glans inflation morphology and female cloaca copulatory interactions of the male American alligator phallus. <i>Biology of Reproduction</i> , 2021, 104, 374-386.	1.2	4
97	A hybrid numeric-analytic solution for pulsed CEST. <i>NMR in Biomedicine</i> , 2022, 35, e4610.	1.6	4
98	Temporal T_1 and relaxation in the rat heart. <i>Magnetic Resonance in Medicine</i> , 2007, 58, 939-946.	1.9	3
99	Diffusion Tensor Tractography Visualizes Partial Nerve Laceration Severity as Early as 1 Week After Surgical Repair in a Rat Model Ex Vivo. <i>Military Medicine</i> , 2020, 185, 35-41.	0.4	3
100	Finite element analysis of bone mechanical properties using MRI-derived bound and pore water concentration maps. <i>Computer Methods in Biomechanics and Biomedical Engineering</i> , 2023, 26, 905-916.	0.9	3
101	Morphological changes associated with Nile crocodile (<i>Crocodylus niloticus</i>) phallic glans inflation. <i>Journal of Morphology</i> , 2020, 281, 636-645.	0.6	2
102	HR-pQCT parameters of the distal radius correlate with the bending strength of the radial diaphysis. <i>Bone</i> , 2022, 161, 116429.	1.4	1
103	Mapping pH using stimulated echoes formed via chemical exchange. <i>Magnetic Resonance Imaging</i> , 2022, 92, 100-107.	1.0	1